HHS Public Access

Author manuscript

Biorheology. Author manuscript; available in PMC 2016 March 30.

Published in final edited form as:

Biorheology. 2015 November 24; 52(5-6): 303–318. doi:10.3233/BIR-15065.

In microfluidico: Recreating *in vivo* hemodynamics using miniaturized devices

Shu Zhu[a], **Bradley A. Herbig**[a], **Ruizhi Li**[a], **Thomas V. Colace**[a], **Ryan W. Muthard**[a], **Keith B. Neeves**[b], and **Scott L. Diamond**[a,*]

[a]Institute for Medicine and Engineering, Department of Chemical and Biomolecular Engineering, University of Pennsylvania, Philadelphia, PA, USA

[b]Department of Chemical and Biomolecular Engineering, Colorado School of Mines, Golden, CO, USA

Abstract

Microfluidic devices create precisely controlled reactive blood flows and typically involve: (i) validated anticoagulation/pharmacology protocols, (ii) defined reactive surfaces, (iii) defined flow-transport regimes, and (iv) optical imaging. An *8-channel device* can be run at constant flow rate or constant pressure drop for blood perfusion over a patterned collagen, collagen/kaolin, or collagen/tissue factor (TF) to measure platelet, thrombin, and fibrin dynamics during clot growth. A *membrane-flow device* delivers a constant flux of platelet agonists or coagulation enzymes into flowing blood. A *trifurcated device* sheaths a central blood flow on both sides with buffer, an ideal approach for on-chip recalcification of citrated blood or drug delivery. A *side-view device* allows clotting on a porous collagen/TF plug at constant pressure differential across the developing clot. The core-shell architecture of clots made in mouse models can be replicated in this device using human blood. For pathological flows, a *stenosis device* achieves shear rates of >100,000 s^{-1} to drive plasma von Willebrand factor (VWF) to form thick long fibers on collagen. Similarly, a *micropost-impingement device* creates extreme elongational and shear flows for VWF fiber formation without collagen. Overall, microfluidics are ideal for studies of clotting, bleeding, fibrin polymerization/fibrinolysis, cell/clot mechanics, adhesion, mechanobiology, and reaction-transport dynamics.

Keywords

Harry Goldsmith; microfluidics; hemorheology; platelet; von Willebrand factor

1. Introduction

The *in vivo* cardiovasculature achieves robust oxygen delivery by pumping blood from the heart to the smallest of capillaries. Composed of diverse cell types, blood flows through a branched and flexible geometry of living vessels. Biorheological complexity arises from single protein and protein ensemble mechanics, single cell biomechanics, dense suspensions

*Address for correspondence: Scott L. Diamond, 3340 Smith Walk, 1020 Vagelos Lab, Philadelphia, PA 19104, USA. Fax: +1 215 573 7227; sld@seas.upenn.edu.

of cells in time-dependent flows, and cellular mechanobiological response to forces transmitted by and through fluids and tissues. In contrast, the *in vitro* setting, once a single glass dish (now plastic), is a sterile environment lacking both flow and forces, which has at least progressed to the 96-well plate format and beyond. Bridging these two extremes is the *in microfluidico* setting that combines flow and high replicates at small length scales to recreate biochemical and biological complexity under the dynamic conditions of the vasculature. The capability of soft lithography [1] to pattern a wafer with micron-scale features and then rapidly imprint that topography on a polydimethylsiloxane (PDMS) polymer has created new and diverse opportunities for biorheological research with blood. In contrast to traditional well plate based studies in which flow and blood cellular constituents are often eliminated, microfluidic devices allow for the development and simultaneous observation of thrombotic events on well-defined prothrombotic surfaces under precisely controlled flow conditions with human whole blood. Many thrombotic events can be accommodated on a single device, thus permitting highly-paralleled whole blood studies without requiring large volumes of whole blood sample from human subjects. Microfluidic devices typically involve a sandwich of the PDMS-molded component held against a glass slide by direct bonding, vacuum sealing, or mechanical clamping. Many recent *in microfluidico* studies are built upon a foundation established by Dr. Harry Goldsmith and collaborators, often published in *Biorheology* [2–6], that emphasizes: (i) precisely controlled flow fields, (ii) high spatial and temporal resolution imaging of flow and single cell motions, and (iii) molecularly-defined biological pathways.

Microfluidic channels are typically square or rectangular, thus creating complex three-dimensional flows especially near the corners of the channel where the flow is completely non-physiological. Using channels that have a high aspect ratio allow the central portion of the flow field to approximate a parallel-plate flow [7,8] by neglecting effects at the side walls and corners. Under these conditions, a cell-free layer is formed near the wall that is enriched in platelets and depleted of red blood cells. In fact, extreme geometries allow skimming of the cell free layer to separate plasma or platelet rich plasma [9], especially with partially-diluted blood.

For blood research, the microfluidic device can be considered an “open” reactor system that contains a small reservoir on or off the device from which blood flows directly into the microfluidic channel(s). Although blood is stable while held by the perfect *in vivo* container (the endothelium), it should be considered perturbed when it is obtained by phlebotomy and delivered to the reservoir of the device. Using fresh human blood *ex vivo* in flow experiments requires precise consideration of anticoagulation so that the blood is minimally perturbed prior to introduction into the microfluidic channel. For coagulation research in which blood generates thrombin, several triggers should be considered and controlled: (i) air/biomaterial activation of the contact pathway (Factor XIIa [FXIIa] generation), (ii) platelet dependent activation of the contact pathway (via polyphosphate release and other FXII activators), (iii) extrinsic activation by endogenous tissue factor (TF, from phlebotomy or from a disease state in the donor) or exogenous TF added by the experimentalist to the reservoir or affixed to the surface of the microchannel (Fig. 1(A)). Numerous inhibitors and experimental designs allow control of these pathways to obtain clotting conditions that range from the contact pathway dominated to the extrinsic pathway dominated (Fig. 1(B)) [10,11].

Due to small length scales within microfluidic devices, *in microfluidico* hemodynamic flows are generally at low Reynolds numbers (Re). In fact, rather extreme geometries are required to create boundary layer separation/impinging flow reattachment [12] in an effort to mimic laminar recirculation zones distal of a coronary stenosis (often described imprecisely as *"disturbed flow"* and incorrectly as turbulent). True fluid mechanical turbulence can be generated in blood in rare circumstances of arteriovenous fistulas, extreme stenosis, or mechanical heart valves. However, turbulence is extremely difficult to create using microfluidic devices due to the micron length scales that keep Re < 10–100.

We describe six different devices that recreate relevant physiological and pathological conditions *in microfluidico* to reveal the biorheology and transport complexity of human blood. These devices have allowed an exploration of platelet activation and adhesion and coagulation under flow, clot permeation and clot retraction, calcium ion transport, and VWF molecular mechanics and biorheology.

2. Material and methods

2.1. Inhibitors and activators

Sodium citrate, a calcium chelating reagent, is typically used as anticoagulant to inhibit calcium dependent mechanisms in the coagulation cascade [13]. Clotting resumes upon recalcification prior to flow into the microfluidic device. However, FXII activation can proceed in the absence of calcium and prime the contact pathway. Because resting time of citrated blood is often an uncontrolled variable, corn trypsin inhibitor (CTI), a β-FXIIa inhibitor at a low level of 4 μg/ml can be used to study the contact pathway by providing partial blockade of contact activation during blood collection but still allowing FXIIa generation on a prothrombotic surface. High level of CTI (40–100 μg/ml) provides strong blockade of β-FXIIa thus allowing the study of the extrinsic pathway. CTI at high concentrations may have some activity on Factor XIa (FXIa) [14,15]. Antibodies such as 14E11 prevent activation of FXI by FXIIa and are analogous to CTI in their use [16–18]. For either CTI or 14E11, thrombin can still feedback activate FXI to FXIa. Antibodies against FXI/FXIa that prevent activation of Factor IX (of the intrinsic tenase Factor IXa/Factor VIIIa) eliminate both the contact pathway and the thrombin feedback activation of FXI, replicating a FXI-deficiency (hemophilia C). A procoagulant surface can be created in the microchannel by patterning collagen which causes platelet activation via GPVI and mediates adhesion through activated platelet integrin $\alpha_2\beta_1$ [7,19,20]. Addition of kaolin to collagen will enhance contact activation of FXII [10], while addition of lipidated TF to collagen (0.1 to 10 molecules/μm^2) [21–23] spans the relevant dose-response regime for triggering the extrinsic pathway. Use of direct Factor Xa or thrombin inhibitors (e.g. 1 μM apixaban or 100 μM D-Phenylalanyl-prolyl-arginyl Chloromethyl Ketone [PPACK], respectively) prevent clotting and allow the study of platelet, red blood cell, and neutrophil function in flowing whole blood without the confounding influence of thrombin and fibrin. Additionally, pharmacological modulators of clotting (recombinant Factor VIIa, anti-tissue factor pathway inhibitor antibody) [24] or platelet activation (aspirin, $P2Y_{12}$ inhibitors, protease activated receptor-1 inhibitors) can be used as part of the experimental design [10,25–27].

2.2. Microfluidic device fabrication

Microfluidic devices were fabricated by soft lithography with PDMS. Photomasks were designed in computer-aided design programs (i.e. DraftSight and LayoutEditor) and were sent for manufacture at OutputCity (Bandon, OR). Designed features on photomasks were then transferred onto silicon wafers using standard photolithograph [1]. PDMS prepolymer and curing reagent (Dow Corning, Midland, MI) were mixed and then degassed under vacuum and cured over the master wafers at 65°C for 3 h. After cooling, the molded PDMS were peeled off and cut into individual devices. Fluidic and vacuum ports were added using Harris Uni-Core (Ted Pells, Inc., Redding, CA). Prior to use, PDMS devices were cleaned in 1N hydrochloric acid followed by immersion in acetone and subsequently ethanol for 15 min each in an ultrasonic cleaning bath. For membrane devices, a polycarbonate membrane with 0.4–1 μm pores was sandwiched between two pieces of PDMS by vacuum bonding [28].

2.3. Defined surfaces for platelet/coagulation studies

Neeves et al. [7] demonstrated the technique of patterning collagen onto glass surface with a single channel PDMS device. Briefly, a drop of collagen type I (Chrono-Log, Havertown, PA) was placed on the inlet port and pulled across the channel of the patterning device with a blunt needle attached to a syringe inserted in the outlet port, followed by a bovine serum albumin (0.5%) washing step. This technique can be applied to generate focal thrombosis within defined prothrombotic regions. In fact, surface-immobilized collagen fibrils not only activate platelets and support platelet aggregation but also serve as substrates for other hemostatically active proteins and/or particles. Colace et al. [21] linked TF-incorporated lipid liposomes to collagen surfaces by biotin-avidin interactions to create defined prothrombotic surfaces mimicking *in vivo* injuries. Zhu et al. [10] utilized electrostatic interactions to decorate collagen surfaces with kaolin (a FXII activator) nanoparticles or lipidated-TF that can trigger thrombin generation via the contact pathway or via both the contact and the extrinsic pathways.

2.4. Detection of platelets, thrombin, and fibrin

Blood was collected via venipuncture from healthy donors into anticoagulants and was immediately transferred into labeling tubes in which it was labeled with fluorescently-conjugated anti-CD41 or CD61 antibody (BD Biosciences, San Jose, CA) and fluorescently-conjugated fibrinogen from human plasma (Life Tech, Carlsbad, CA) for platelet and fibrin detection, respectively. To detect thrombin, a thrombin-sensitive platelet-targeting sensor was added to blood prior to perfusion. This sensor was made up of a thrombin-sensitive peptide with a thrombin-releasable quencher that was linked to an anti-CD61 antibody ensuring its incorporation into thrombi [29]. The labeled whole blood was subsequently transferred to the microfluidic device and perfused over pre-patterned prothrombotic surfaces under controlled shear conditions via a syringe pump connected to the outlet of the device. Platelet aggregation, fibrin, and thrombin generation within the focal collagen region was then simultaneously monitored via epifluorescence microscopy (IX81, Olympus, Center Valley, PA). Images were captured using a charge-coupled device digital camera

(Hamamatsu, Bridgewater, NJ). All acquired images were processed using ImageJ (National Institute of Health).

2.5. Simulation model

To calculate the flow conditions in the microfluidic devices, the device geometries were constructed in the fluid dynamics simulation program COMSOL Multiphysics (Burlington, MA). Fluid properties and inlet and outlet flow rates or pressures were defined in COMSOL. The program then calculated the velocity, pressure, and shear rate at each point within the defined channel geometry based on the specified input conditions. These simulated values were used in the design of microfluidic experiment, for example, in calculating the necessary flow rate to achieve a particular local shear rate in the device.

3. Results

3.1. The 8-channel device

A microfluidic device that consists of 8 flow channels was developed by Maloney et al. in 2010 [19], which was subsequently used in several works to generate focal thrombosis on micro-patterned collagen surfaces [10,11,21,22,24–26,30] (Fig. 2(A)). By varying the surface TF concentration and the anticoagulants added during blood collection, thrombin generation on patterned surfaces can be driven primarily by the contact pathway, the extrinsic pathway, or by some combination of both pathways. Zhu et al. had shown in a recent study that FXI antibodies 14E11 and O1A6 were only effective for thrombin inhibition at low TF levels (<~0.2 molecules/μm^2) at a venous shear rate (100 s^{-1}) where the contact pathway and the FXI-dependent thrombin amplification mechanism could overcome the extrinsic pathway [11]. An extrinsic pathway dominating collagen/high TF (~5–10 molecules/μm^2) surface was able to vigorously trigger thrombin generation and allow for faster platelet and fibrin onset than that of a collagen surface (Fig. 2(B)–(C)), indicating the stronger potency of TF in triggering thrombin generation under venous shear conditions. Interestingly, fibrin generation on both collagen/kaolin and collagen/TF surfaces was substantially delayed and suppressed at arterial shear rate, suggesting the extrinsic and contact pathways have similar flow sensitivity under arterial shear conditions [10], probably owing to the excessive dilution of coagulation proteins by flow.

The vast majority of microfluidic models used to study the hemostatic mechanism under relevant local wall shear rate conditions are driven by constant flow rate (Const Q) syringe pumps. Instead, the *in vivo* pump, the heart, operates to create arterial pressure to drive flow. In 2012 Colace et al. [22] demonstrated that a platelet/fibrin aggregate depositing under Const Q in a fixed volume experiences a nonlinear increase in local wall shear rate as the clot grow (Fig. 2(C)) whereas a platelet/fibrin mass forming under constant pressure drop conditions (Const ΔP) experiences an initial increase in local wall shear rate followed by a decline (Fig. 2(D)), caused by a decrease in flow rate during the formation of the thrombus (Fig. 2(D), bottom panel). The authors were able to achieve Const Q vs. Const ΔP conditions by employing the 8-channel flow device. Under Const Q conditions whole blood was run through all 8 channels, while under Const ΔP conditions, channels with whole blood were staggered with channels of whole blood treated with ethylenediaminetetraacetic acid

(EDTA) to chelate Ca^{2+}, an essential component of platelet adhesion. Platelet/fibrin masses formed under Const Q conditions grew more rapidly than those under Const ΔP, perhaps due to increased VWF function under increased shear rate [31] and always ruptured (formed *in vitro* emboli, Fig. 2(C)) from the pro-aggregatory surface. Those *in vitro* thrombi developed under Const ΔP conditions, however, grew to fully occlude their containing vessels and diverted flow through the EDTA containing channels (Fig. 2(D)). The Const ΔP mode is the more physiological relevant mode of operation; in which thrombotic occlusion can be achieved by diverting flow to a paired open channel. However, under this operation mode, the requirement of pressure relieving channels reduced the availability of the assay channels on a single device, which can be potentially changed by employing a pressure sensing and controlling system in each channel.

Local hemodynamic conditions around a developing microfluidic thrombus can be calculated using both two-dimensional and three-dimensional COMSOL models in conjunction with epifluorescence microscopy to quantify platelet and fibrin deposition. When whole blood was treated with Gly-Pro-Arg-Pro (GPRP), a peptide inhibitor of fibrin polymerization, the resulting thrombi were unable to withstand local wall shear rates of 2,900 s^{-1} (Fig. 2(C) and (D), *open circles*). Although fibrin, the polymeric protein that weaves a tight mesh around platelet aggregates, was already believed to provide clots with structure [32], this study was the first to quantify a dramatic increase in the shear resistance of clots formed with fibrin as opposed to those formed in the presence of GPRP.

This 8-channel device allowed for simultaneous evaluation of platelet responsiveness to multiple inhibitors under precisely controlled surface and hemodynamic conditions without requiring large volume of whole blood. This high-throughput microfluidic thrombosis model has been used to evaluate platelet function and coagulation from patients with congenital bleeding disorders [24,30].

3.2. Membrane-flow device

The generation of platelet agonists and thrombin regulate platelet activation and aggregation, as well as fibrin deposition. Under hemodynamic conditions, these soluble molecules are subject to transport limitations due to delivery to and dilution from an injury site. However, there are few ways to experimentally control wall fluxes of agonists into flowing blood or blood constituents. To address this technology gap, a membrane microfluidic device was developed consisting of two microfluidic channels running perpendicular to each other, separated by a membrane (Fig. 3(A)). The wall shear rate and wall solute flux can be independently manipulated by the pressure gradient across the channel and the transmembrane pressure, respectively. A concentration boundary layer is formed at the intersection of the two channels where platelet deposition can be monitored by fluorescence. For example, adenosine diphosphate (ADP) was introduced into whole blood flowing at 250 s^{-1}. The degree of platelet aggregation induced by ADP ranged from none to monolayers to multilayer aggregates over the fluxes of 1.5–4.4 × 10^{-9} nmol $\mu m^{-2}s^{-1}$ [33]. These data show that small changes in local agonist concentrations can have a profound effect on platelet aggregate size. The membrane device was also used to define the state diagram for fibrin deposition and morphology under flow [28]. Here, thrombin (10^{-13}–10^{-11} nmol $\mu m^{-2}s^{-1}$)

was introduced into flowing fibrinogen (10–100 s^{-1}) and compared to theoretical reactiontransport models of fibrin polymerization. A fibrin morphology state diagram was defined by the Peclet (Pe) and Dahmköhler (Da) numbers; where Da < 10 yielded thin films or sheets of fibrin with no perceptible fibers, 10 < Da < 900 gave two-dimensional mats of fibers, and Da > 900 and Pe < 100 gave three-dimensional gels. These results show that transport limitations to fibrin assembly first inhibit lateral aggregation and then protofibrils extension. Importantly, these data also suggest that it is exceedingly difficult to form fibrin at shear rates greater than 100 s^{-1} without protection by adhered blood cells or other topological features from the dilution effect of blood flow.

This membrane device was the first enabling control of the flux of platelet agonists into flowing whole blood. It is a valuable tool for elucidating the importance of platelet agonists and possibly endothelium secreted soluble molecules on clot formation and stability. However, potential membrane fouling causing a reduction in agonist flux could be a challenge in long-term experiments.

3.3. Side-view device

Subendothelial matrix proteins such as collagen and TF are exposed to flowing whole blood following vascular injury. Platelets and coagulation factors must overcome the local hemodynamic conditions of the injury to develop a stable non-occlusive clot. The two hemodynamic conditions that govern thrombus development are wall shear rate and the pressure gradient between the vessel lumen and extravascular tissue. In order to study the effect of these parameters on spatiotemporal clot growth, Muthard and Diamond designed a side-view microfluidic device capable of independently controlling both wall shear rate and pressure gradient across developing thrombi (Fig. 4(A)) [34]. The authors were able to use this device to experimentally determine the permeability of clots developed under physiologic flow and pressure conditions. Interestingly, platelet/fibrin clots had a permeability of $\kappa = 2.71 \times 10^{-14}$ cm^2, nearly ~730-fold less permeable than collagen alone. In addition, the side-view design of the device also enabled the authors to study the effects of pressure gradient across developing thrombi on platelet and thrombin boundary layer growth at arterial shear stresses [35]. When the pressure-driven permeation across the clot was increased by applying a pressure gradient ($\Delta P = 23.4$ mmHg) across the clot, thrombin was rapidly convected through the clot, demonstrated by a 62% decrease in thrombin fluorescent intensity inside the thrombus. These studies led Muthard et al. to investigate the differences in activation gradients inside clots at both physiologic (venous and arterial) and pathologic shear rates (>10,000 s^{-1}) [36]. The clots generated within the side-view microfluidic device displayed activation gradients within the thrombi that mimicked *in vivo* clots generated in mice (Fig. 4(B) and (C)) [37]. Highly-activated regions of P-selectin positive platelets occupied the “core” region of the clot where the majority of thrombin activity was observed. These results demonstrated the ability of the side-view microfluidic device to recreate the hemodynamic conditions found throughout the vasculature.

This device provided a novel approach to study clot development and permeation under independently controlled wall shear rate and pressure gradient across developing thrombi. The formed clots are visualized from the side, which is similar with the view of intravital

microscopy in the mouse laser injury models, thus providing results acquired with human whole blood under physiological mimicking flow conditions that are comparable to results from animal laser injury models.

3.4. Trifurcated device

During blood collection in a clinical setting, anticoagulation with sodium citrate extends the time in which the blood sample can be accurately tested. Recalcification of citrated blood provides the user with the ability to initiate platelet and coagulation function just prior to beginning their testing. This approach can be extremely beneficial if the same recalcification routine is used across different blood testing sites. Unfortunately different recalcification concentrations and wait times can drastically change assay results. In order to eliminate this variability, Muthard and Diamond designed a trifurcated microfluidic device that rapidly recalcifies citrated whole blood under a constant wall shear rate [38]. The device uses three channels to sheath a blood flow in a viscous calcium buffer (Fig. 5(A)). The authors patterned collagen ± TF perpendicular to the blood flow path downstream of the trifurcated entrance. Using fluorescent antibodies to visualize platelet and fibrin (ogen) formation, the localized clotting events were imaged dynamically to investigate proper recalcification of the citrated sample (Fig. 5(B)). Without recalcification via the calcium buffer sheath, platelet and coagulation function were completely abolished (Fig. 5(C)).

This trifurcated device demonstrated the ability to effectively provide a consistent delivery of recalcification buffer or investigate drug dosing at varying levels of recalcification in a single channel. In addition to recalcification, this device can also be used for control of temperature, pH and hematocrit, making it a useful tool for the investigation of the effects of hypothermia, acidosis, and hematocrit on platelet function and coagulation.

3.5. Stenosis device

VWF is a large polymeric protein found in blood, within platelets and endothelial cells, and the vessel wall. It is believed that the primary role of collagen-bound VWF present in the vessel wall is to slow platelets through a fast-on/fast-off interaction with platelet receptor GPIb [39]. Soluble VWF is a shear-sensitive molecule [40]. Upon exposure to shear rates in excess of 5,000 s^{-1}, VWF may unfold into an elongated conformation. This conformation exposes domains of the molecule which enhance its binding to platelet GPIb [41] as well as its proteolysis by ADAMTS13 [42,43]. In patients with severe aortic stenosis or with left ventricular assist devices, conditions which expose blood to pathological shear stresses, a clearance of VWF has been observed, as well as a bleeding tendency [44–47]. The mechanism of VWF clearance is not well understood in these patients. It has been demonstrated that elongated VWF may self-associate and ensnare platelets into large supramolecular complexes *in vitro* [48]. It could be reasoned that if this process occurred *in vivo*, these complexes may be subsequently cleared. In 2013, Colace and Diamond used a microfluidic stenosis model to demonstrate that soluble VWF from platelet poor plasma could deposit onto surfaces of fibrillar collagen type 1 at shear rates of >10,000 s^{-1} (Fig. 6(A)). Furthermore, the authors illustrated that these molecules of VWF were likely to be complexes of self-associated VWF as staining with epifluorescent anti-VWF antibody revealed structures greater than 100 μm in length forming on the collagen matrix (Fig. 6(B)).

VWF appeared in regions of the microfluidic device where the threshold shear rate was reached and was not enhanced by sharp shear rate gradients in either the inlet or outlets to the microfluidic stenosis (Fig. 6(C)).

This stenosis microfluidic device allowed for the study of the high shear rate dependent mechanisms of VWF by mimicking the geometry of an injured stenotic blood vessel. By exposing a collagen surface in this high shear region, the importance of plasma VWF and its interactions with collagen could be explored.

3.6. Micropost-impingement device

Additionally, in 2015, Herbig et al. have studied VWF using an impingement-post microfluidic device, which captures insoluble fibrous VWF in flow from plasma without the potentially confounding use of collagen [49]. Platelet-free plasma was perfused through a rapidly narrowing channel to increase shear rate before flowing over a micropost positioned in flow (Fig. 7(A)). The high shear, narrowed channel polymerizes soluble VWF multimers in plasma at 10,000 s^{-1} and catches the resulting insoluble fibers on the micropost, held in place by fluid forces (Fig. 7(B)). After formation of the VWF fibers, the perfused fluid can be changed to study the mechanics and biology of fibrous VWF.

Distinct from the ultra-large VWF (ULVWF) released from stimulated endothelial cells, fibrous VWF is made up of plasma VWF which has already been processed from the ULVWF form by ADAMTS13 in its release from endothelial cells. The size of the VWF fibers is shear-dependent, with higher shear rates resulting in larger fibers. An estimate for the elastic modulus of fibrous VWF was also found in this device by stretching a small fiber generated on the post, and comparing the stress applied by the fluid at each flow rate to the resulting strain on the fiber. The resulting estimate of 50 MPa is similar to those previously found for fibrin [50] and collagen [51]. Platelet adhesion and activation has also been studied in this device by perfusing whole blood over VWF fibers formed from plasma. As previously observed on ULVWF [52], platelets rolled and firmly attached along the fibers at arterial shear rates utilizing GPIb and $\alpha_{IIb}\beta_3$ respectively. Additionally, shear-induced platelet activation was observed at upstream shear rates of 1,500 s^{-1} and 3,000 s^{-1} using P-selectin as a marker for platelet activation (Fig. 7(C)).

This impingement-post microfluidic device is unique in its ability to isolate VWF fibers from plasma in flow without collagen or edothelium to study VWF's role in thrombosis.

4. Conclusions

Innovative reagents have increased control of blood biochemistry in the *ex vivo* setting (Fig. 1), allowing a number of biological, pharmacological and clinical questions to be studied in specific devices (Figs 2–6). The *in microfluidico* research methodology has become particularly critical to coagulation research [53,54] and to Blood Systems Biology research [55]. Significant progress has been made in linking platelet models [56] to multiscale simulations of platelet deposition under flow, as measured in microfluidic devices [57]. Combining micropatterning with microfluidics has provided a means to measure platelet function and coagulation under flow in a combinatorial manner that approaches that of well-

plate formats [23,58–60]. Endothelial cells cultured within microfluidic devices followed by exposure chemical or thermal activation and flowing whole blood are revealing new rheological- and transport-dependent mechanisms in microvascular diseases [61–63].

New devices, measurements, and models will continue to shape the future of research on blood under flow. These technologies will be applied to understand the kinetics and mechanics of blood clots by exploring platelet actin polymerization, platelet myosin-driven contraction, fibrin rheology, mechanosensing in contracted platelet clots [64], and altered molecular transport in platelet retracted clots. Even the generation of culture-derived platelets from embryonic stem cells, induced pluripotent stem cells, and cord blood has benefited from the design of specialized microfluidic devices [65]. Additional challenges in the future will involve improving microfluidic study of the cell margination in flow, the blood-endothelium interface, the role of inflammation in coagulation and bleeding processes, and molecular mechanics at the single bond and the single molecule level.

In addition to improving the mechanistic understanding of blood, the *in microfluidico* approach can also be used as a way of developing new diagnostic tools for clinical application. The development of pre-manufactured microfluidic devices that are ready for use in the clinical labs would be valuable for decreasing the costs and increasing the speed of clinical blood diagnostics. The advantages described in this review help to demonstrate why new microfluidic approaches have the potential to shape the future of basic science research and clinical diagnostic development.

List of abbreviations

ADP	Adenosine diphosphate
Const Q	Constant flow rate
Const ΔP	Constant pressure drop
CTI	Corn trypsin inhibitor
Da	Dahmköhler number
EDTA	Ethylenediaminetetraacetic acid
FXI/FXIa	Coagulation factor XI/XIa
FXII/FXIIa	Coagulation factor XII/XIIa
GPRP	Gly-Pro-Arg-Pro
PDMS	Polydimethylsiloxane
Pe	Peclet number
PPACK	D-Phenylalanyl-prolyl-arginyl Chloromethyl Ketone
Re	Reynolds number
TF	Tissue factor
ULVWF	Ultra-large von Willebrand factor

VWF	Von Willebrand factor

References

1. Kane RS, Takayama S, Ostuni E, Ingber DE, Whitesides GM. Patterning proteins and cells using soft lithography. Biomaterials. 1999; 20:2363–2376. [PubMed: 10614942]
2. Goldsmith HL. Deformation of human red cells in tube flow. Biorheology. 1971; 7:235–242. [PubMed: 5580364]
3. Goldsmith HL, Bell DN, Spain S, McIntosh FA. Effect of red blood cells and their aggregates on platelets and white cells in flowing blood. Biorheology. 1999; 36:461–468. [PubMed: 10818647]
4. Goldsmith HL, Kaufer ES, McIntosh FA. Effect of hematocrit on adenosine diphosphate-induced aggregation of human platelets in tube flow. Biorheology. 1995; 32:537–552. [PubMed: 8541523]
5. Goldsmith HL, Lichtarge O, Tessier-Lavigne M, Spain S. Some model experiments in hemodynamics: VI. Two-body collisions between blood cells. Biorheology. 1981; 18:531–555. [PubMed: 7326392]
6. Diamond SL, Lawrence MB, Neelamegham S. Harry L. Goldsmith, Ph.D. Ann Biomed Eng. 2008; 36:523–526. [PubMed: 18330702]
7. Neeves KB, Maloney SF, Fong KP, Schmaier AA, Kahn ML, Brass LF, et al. Microfluidic focal thrombosis model for measuring murine platelet deposition and stability: PAR4 signaling enhances shear-resistance of platelet aggregates. J Thromb Haemost. 2008; 6:2193–2201. [PubMed: 18983510]
8. Sarvepalli DP, Schmidtke DW, Nollert MU. Design considerations for a microfluidic device to quantify the platelet adhesion to collagen at physiological shear rates. Ann Biomed Eng. 2009; 37:1331–1341. [PubMed: 19440840]
9. Tripathi S, Prabhakar A, Kumar N, Singh SG, Agrawal A. Blood plasma separation in elevated dimension T-shaped microchannel. Biomed Microdevices. 2013; 15:415–425. [PubMed: 23355067]
10. Zhu S, Diamond SL. Contact activation of blood coagulation on a defined kaolin/collagen surface in a microfluidic assay. Thromb Res. 2014; 134:1335–1343. [PubMed: 25303860]
11. Zhu S, Travers RJ, Morrissey JH, Diamond SL. FXIa and platelet polyphosphate as therapeutic targets during human blood clotting on collagen/tissue factor surfaces under flow. Blood. 2015; 126(12):1494–1502. [PubMed: 26136249]
12. Nesbitt WS, Westein E, Tovar-Lopez FJ, Tolouei E, Mitchell A, Fu J, et al. A shear gradient-dependent platelet aggregation mechanism drives thrombus formation. Nat Med. 2009; 15:665–673. [PubMed: 19465929]
13. Mann KG, Whelihan MF, Butenas S, Orfeo T. Citrate anticoagulation and the dynamics of thrombin generation. J Thromb Haemost. 2007; 5:2055–2061. [PubMed: 17883701]
14. Hansson KM, Nielsen S, Elq M, Deinum J. The effect of corn trypsin inhibitor and inhibiting antibodies for FXIa and FXIIa on coagulation of plasma and whole blood. J Thromb Haemost. 2014; 12:1678–1686. [PubMed: 25142753]
15. Butenas S, Mann KG. The effect of corn trypsin inhibitor and inhibiting antibodies for FXIa and FXIIa on coagulation of plasma and whole blood: Comment. J Thromb Haemost. 2015; 13:487–488. [PubMed: 25523109]
16. Cheng Q, Tucker EI, Pine MS, Sisler I, Matafonov A, Sun M, et al. A role for factor XIIa-mediated factor XI activation in thrombus formation in vivo. Blood. 2010; 116:3981–3989. [PubMed: 20634381]
17. Kravtsov DV, Matafonov A, Tucker EI, Sun MF, Walsh PN, Gruber A, et al. Factor XI contributes to thrombin generation in the absence of factor XII. Blood. 2009; 114:452–458. [PubMed: 19351955]
18. Puy C, Tucker EI,Wong ZC, Gailani D, Smith SA, Choi SH, et al. Factor XII promotes blood coagulation independent of factor XI in the presence of long-chain polyphosphates. J Thromb Haemost. 2013; 11:1341–1352. [PubMed: 23659638]

19. Maloney SF, Brass LF, Diamond SL. P2Y12 or P2Y1 inhibitors reduce platelet deposition in a microfluidic model of thrombosis while apyrase lacks efficacy under flow conditions. Integr Biol. 2009; 2:183–192.
20. Colace T, Falls E, Zheng XL, Diamond SL. Analysis of morphology of platelet aggregates formed on collagen under laminar blood flow. Ann Biomed Eng. 2011; 39:922–929. [PubMed: 20949319]
21. Colace TV, Jobson J, Diamond SL. Relipidated tissue factor linked collagen surfaces potentiates platelet adhesion and fibrin formation in a microfluidic model of vessel injury. Bioconjug Chem. 2011; 22:2104–2109. [PubMed: 21902184]
22. Colace TV, Muthard RW, Diamond SL. Thrombus growth and embolism on tissue factor-bearing collagen surfaces under flow: Role of thrombin with and without fibrin. Arterioscler Thromb Vasc Biol. 2012; 32:1466–1476. [PubMed: 22516070]
23. Okorie UM, Denney WS, Chatterjee MS, Neeves KB, Diamond SL. Determination of surface tissue factor thresholds that trigger coagulation at venous and arterial shear rates: Amplification of 100 fM circulating tissue factor requires flow. Blood. 2008; 111:3507–3513. [PubMed: 18203955]
24. Li R, Panckeri KA, Fogarty PF, Diamond SL. Recombinant factor VIIa enhances platelet deposition from flowing haemophilic blood but requires the contact pathway to promote fibrin deposition. Haemophilia. 2015; 21:266–274. [PubMed: 25311576]
25. Li R, Diamond SL. Detection of platelet sensitivity to inhibitors of COX-1, P2Y1, and P2Y12 using a whole blood microfluidic flow assay. Thromb Res. 2014; 133:203–210. [PubMed: 24365044]
26. Li R, Fries S, Li X, Grosser T, Diamond SL. Microfluidic assay of platelet deposition on collagen by perfusion of whole blood from healthy individuals taking aspirin. Clin Chem. 2013; 59:1195–1204. [PubMed: 23592503]
27. Li X, Fries S, Li R, Lawson JA, Propert KJ, Diamond SL, et al. Differential impairment of aspirin-dependent platelet cyclooxygenase acetylation by nonsteroidal antiinflammatory drugs. Proc Natl Acad Sci USA. 2014; 111:16830–16835. [PubMed: 25385584]
28. Neeves KB, Illing DA, Diamond SL. Thrombin flux and wall shear rate regulate fibrin fiber deposition state during polymerization under flow. Biophys J. 2010; 98:1344–1352. [PubMed: 20371335]
29. Welsh JD, Colace TV, Muthard RW, Stalker TJ, Brass LF, Diamond SL. Platelet-targeting sensor reveals thrombin gradients within blood clots forming in microfluidic assays and in mouse. J Thromb Haemost. 2012; 10:2344–2353. [PubMed: 22978514]
30. Colace TV, Fogarty PF, Panckeri KA, Li R, Diamond SL. Microfluidic assay of hemophilic blood clotting: Distinct deficits in platelet and fibrin deposition at low factor levels. J Thromb Haemost. 2014; 12:147–158. [PubMed: 24261634]
31. Shankaran H, Alexandridis P, Neelamegham S. Aspects of hydrodynamic shear regulating shear-induced platelet activation and self-association of von Willebrand factor in suspension. Blood. 2003; 101:2637–2645. [PubMed: 12456504]
32. Wolberg AS, Campbell RA. Thrombin generation, fibrin clot formation and hemostasis. Transfus Apher Sci. 2008; 38:15–23. [PubMed: 18282807]
33. Neeves KB, Diamond SL. A membrane-based microfluidic device for controlling the flux of platelet agonists into flowing blood. Lab Chip. 2008; 8:701–709. [PubMed: 18432339]
34. Muthard RW, Diamond SL. Blood clots are rapidly assembled hemodynamic sensors: Flow arrest triggers intraluminal thrombus contraction. Arterioscler Thromb Vasc Biol. 2012; 32:2938–2945. [PubMed: 23087356]
35. Muthard RW, Diamond SL. Side view thrombosis microfluidic device with controllable wall shear rate and transthrombus pressure gradient. Lab Chip. 2013; 13:1883–1891. [PubMed: 23549358]
36. Muthard RW, Welsh JD, Brass LF, Diamond SL. Fibrin, γ′-fibrinogen, and transclot pressure gradient control hemostatic clot growth during human blood flow over a collagen/tissue factor wound. Arterioscler Thromb Vasc Biol. 2015; 35:645–654. [PubMed: 25614284]
37. Stalker TJ, Traxler EA, Wu J, Wannemacher KM, Cermignano SL, Voronov R, et al. Hierarchical organization in the hemostatic response and its relationship to the platelet-signaling network. Blood. 2013; 121:1875–1885. [PubMed: 23303817]

38. Muthard RW, Diamond SL. Rapid on-chip recalcification and drug dosing of citrated whole blood using microfluidic buffer sheath flow. Biorheology. 2014; 51:227–237. [PubMed: 24898333]
39. Doggett TA, Girdhar G, Lawshe A, Schmidtke DW, Laurenzi IJ, Diamond SL, et al. Selectin-like kinetics and biomechanics promote rapid platelet adhesion in flow: The GPIb(alpha)-vWF tether bond. Biophys J. 2002; 83:194–205. [PubMed: 12080112]
40. Barg A, Ossig R, Goerge T, Schneider MF, Schillers H, Oberleithner H, et al. Soluble plasma-derived von Willebrand factor assembles to a haemostatically active filamentous network. Thromb Haemost. 2007; 97:514–526. [PubMed: 17393012]
41. Dayananda KM, Singh I, Mondal N, Neelamegham S. VonWillebrand factor self-association on platelet GpIbalpha under hydrodynamic shear: Effect on shear-induced platelet activation. Blood. 2010; 116:3990–3998. [PubMed: 20696943]
42. Zhang X, Halvorsen K, Zhang CZ, Wong WP, Springer TA. Mechanoenzymatic cleavage of the ultralarge vascular protein von Willebrand factor. Science. 2009; 324:1330–1334. [PubMed: 19498171]
43. Xu AJ, Springer TA. Calcium stabilizes the von Willebrand factor A2 domain by promoting refolding. Proc Natl Acad Sci USA. 2012; 109:3742–3747. [PubMed: 22357761]
44. Vincentelli A, Susen S, Le Tourneau T, Six I, Fabre O, Juthier F, et al. Acquired von Willebrand syndrome in aortic stenosis. N Engl J Med. 2003; 349:343–349. [PubMed: 12878741]
45. Uriel N, Pak SW, Jorde UP, Jude B, Susen S, Vincentelli A, et al. Acquired von Willebrand syndrome after continuous-flow mechanical device support contributes to a high prevalence of bleeding during long-term support and at the time of transplantation. J Am Coll Cardiol. 2010; 56:1207–1213. [PubMed: 20598466]
46. Geisen U, Heilmann C, Beyersdorf F, Benk C, Berchtold-Herz M, Schlensak C, et al. Non-surgical bleeding in patients with ventricular assist devices could be explained by acquired von Willebrand disease. Eur J Cardiothorac Surg. 2008; 33:679–684. [PubMed: 18282712]
47. Pareti FI, Lattuada A, Bressi C, Zanobini M, Sala A, Steffan A, et al. Proteolysis of von Willebrand factor and shear stress-induced platelet aggregation in patients with aortic valve stenosis. Circulation. 2000; 102:1290–1295. [PubMed: 10982545]
48. Reininger AJ, Heijnen HF, Schumann H, Specht HM, Schramm W, Ruggeri ZM. Mechanism of platelet adhesion to von Willebrand factor and microparticle formation under high shear stress. Blood. 2006; 107:3537–3545. [PubMed: 16449527]
49. Herbig BA, Diamond SL. Pathological von Willebrand factor fibers resist tissue plasminogen activator and ADAMTS13 while promoting the contact pathway and shear-induced platelet activation. J Thromb Haemost. 2015; 13(9):1699–1708. [PubMed: 26178390]
50. Collet J-P, Shuman H, Ledger RE, Lee S, Weisel JW. The elasticity of anindividual fibrin fiber in a clot. Proc Natl Acad Sci USA. 2005; 102:9133–9137. [PubMed: 15967976]
51. Grant CA, Brockwell DJ, Radford SE, Thomson NH. Tuning the elastic modulus of hydrated collagen fibrils. Biophys J. 2009; 97:2985–2992. [PubMed: 19948128]
52. Fredrickson BJ, Dong JF, McIntire LV, Lopez JA. Shear-dependent rolling on von Willebrand factor of mammalian cells expressing the platelet glycoprotein Ib-IX-V complex. Blood. 1998; 92:3684–3693. [PubMed: 9808562]
53. Colace TV, Tormoen GW, McCarty OJ, Diamond SL. Microfluidics and coagulation biology. Annu Rev Biomed Eng. 2013; 15:283–303. [PubMed: 23642241]
54. Fogelson AL, Neeyes KB. Fluid mechanics of blood clot formation. Annu Rev Fluid Mech. 2015; 47:377–403. [PubMed: 26236058]
55. Diamond SL. Systems biology of coagulation. J Thromb Haemost. 2013; 11(Suppl 1):224–232. [PubMed: 23809126]
56. Chatterjee MS, Purvis JE, Brass LF, Diamond SL. Pairwise agonist scanning predicts cellular signaling responses to combinatorial stimuli. Nat Biotechnol. 2010; 28:727–732. [PubMed: 20562863]
57. Flamm MH, Colace TV, Chatterjee MS, Jing H, Zhou S, Jaeger D, et al. Multisclae prediction of patient-specific platelet function under flow. Blood. 2012; 120:190–198. [PubMed: 22517902]
58. Okorie UM, Diamond SL. Matrix protein microarrays for spatially and compositionally controlled microspot thrombosis under laminar flow. Biophys J. 2006; 91:3474–3481. [PubMed: 16905604]

59. Hansen RR, Wufsus AR, Barton ST, Onasoga AA, Johnson-Paben RM, Neeves KB. High content evaluation of shear dependent platelet function in a microfluidic flow assay. Ann Biomed Eng. 2013; 41:250–262. [PubMed: 23001359]

60. deWitt SM, Swieringa F, Cavill R, Lamers MM, van Kruchten R, Mastenbroek T, et al. Identification of platelet function defects by multi-parameter assessment of thrombus formation. Nat Commun. 2014; 5:4257. [PubMed: 25027852]

61. Zheng Y, Chen J, Craven M, Choi NW, Totorica S, Diaz-Santana A, et al. In vitro microvessels for the study of angiogenesis and thrombosis. Proc Natl Acad Sci USA. 2012; 109:9342–9347. [PubMed: 22645376]

62. Tsai M, Kita A, Leach J, Rounsevell R, Huang JN, Moake J, et al. In vitro modeling of the microvascular occlusion and thrombosis that occur in hematologic diseases using microfluidic technology. J Clin Invest. 2012; 122:408–418. [PubMed: 22156199]

63. Sylman JL, Artzer DT, Rana K, Neeves KB. A vascular injury model using focal heat-induced activation of endothelial cells. Integr Biol (Camb). 2015; 7:801–814. [PubMed: 26087748]

64. Qiu Y, Brown AC, Myers DR, Sakurai Y, Mannino RG, Tran R, et al. Platelet mechanosensing of substrate stiffness during clot formation mediates adhesion, spreading, and activation. Proc Natl Acad Sci USA. 2014; 111:14430–14435. [PubMed: 25246564]

65. Thon JN, Mazutis L, Wu S, Sylman JL, Ehrlicher A, Machlus KR, et al. Platelet bioreactor-on-a-chip. Blood. 2014; 124:1857–1867. [PubMed: 25606631]

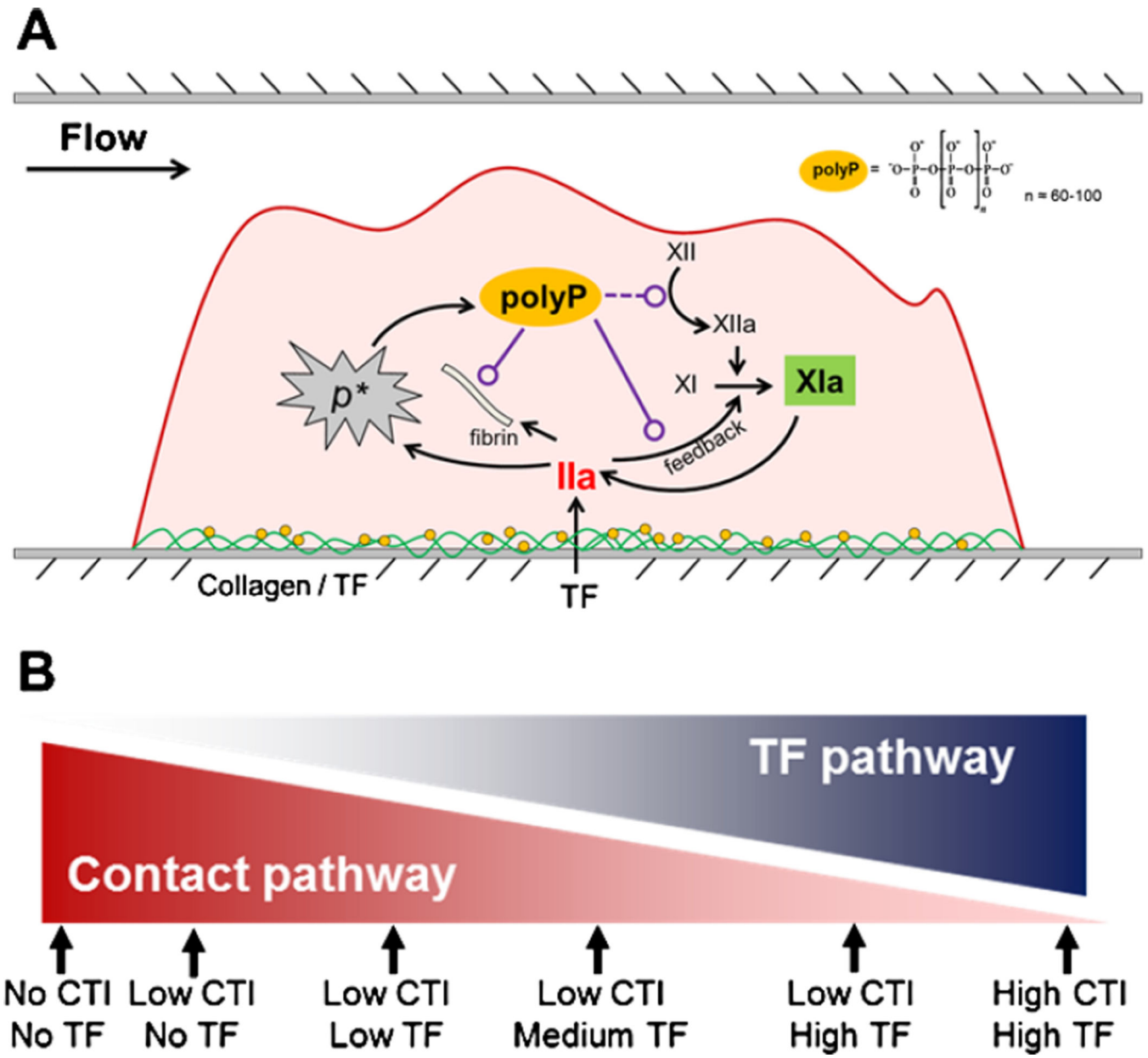

Fig. 1.

The initiation and pharmacological regulation of thrombin production and coagulation using whole blood in microfluidic devices. Pre-patterned collagen/TF surface can simultaneously trigger thrombin generation and support platelet aggregation. As thrombi builds up, packed activated platelets secret high concentration of polyphosphate (polyP), which promotes contact activation and thrombin feedback activation of FXI and enhances fibrin physical structure (A). By varing TF surface concentration and CTI concentration used for anticoagulation, Zhu et al. [11] generated various coagulation conditions (B) under which thrombin generation can be primarily dominated by the contact pathway (low/no CTI, no TF) or the extrinsic pathway (high/low CTI, high TF) or regulated by both pathways with

comparable contributions (low CTI, low–medium TF). (Colors are visible in the online version of the article; http://dx.doi.org/10.3233/BIR-15065.)

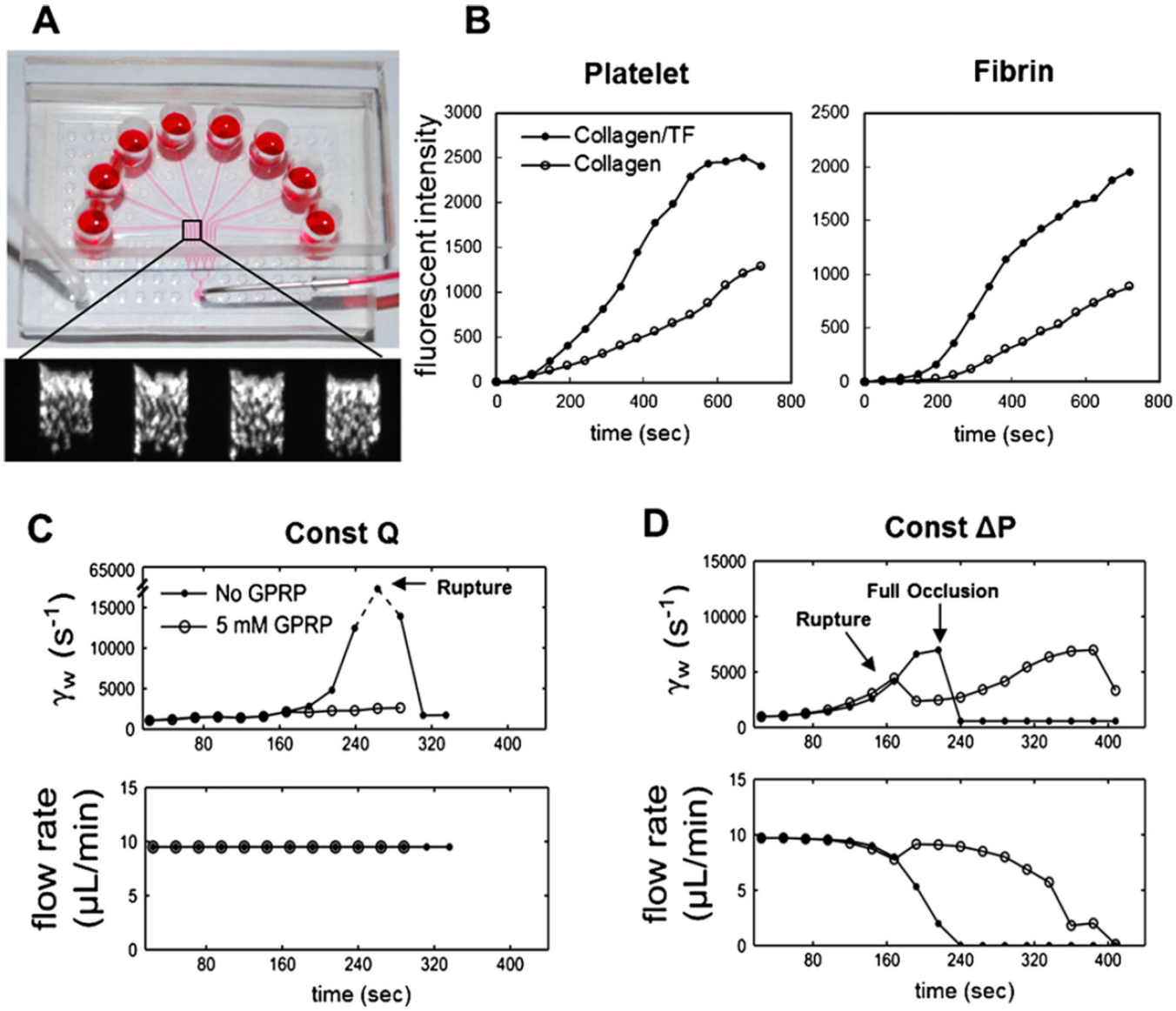

Fig. 2.

8-channel device. A microfluidic device consisting of 8 separate inlets perfused by a single outlet (A, top). This device can be run under Const Q by perfusing all 8 channels with whole blood or under Const ΔP by staggering channels of whole blood with channels of whole blood treated with EDTA to prevent platelet deposition. The bottom panel illustrates 4 platelet masses (of 8) depositing in parallel under whole blood perfusion at 1,000 s^{-1} at Const Q (platelets were labeled with a fluorescently tagged antibody). The channel width is 250 μm. At Const Q, when whole blood was perfused over collagen surface at 100 s^{-1}, both platelet aggregation and fibrin formation were promoted in the presence of high level of surface immobolized TF (~5–10 molec/μm^2) (B). In Colace et al. [22], local wall shear rate was calculated using a two-dimensional COMSOL model at a representative platelet surface by assuming that the aggregate height was proportional to its epifluorescence. Platelet/fibrin masses (closed circles) experienced an increase in shear rate until rupture. Samples treated

with GPRP to inhibit fibrin formation (open circles) did not withstand shear rates greater than 2,900 s^{-1} (C). Platelet/fibrin masses formed under Const ΔP experienced a biphasic local wall shear rate profile. When aggregates approached 75% of full channel occlusion, a steep drop in channel flow rate was calculated. A representative samples treated with GPRP (open circles) began to occlude the channel but ruptured at ~150 s and organized into a more hemodynamically favorable conformation such that the local wall shear rates could not be accurately predicted (D). (Colors are visible in the online version of the article; http://dx.doi.org/10.3233/BIR-15065.)

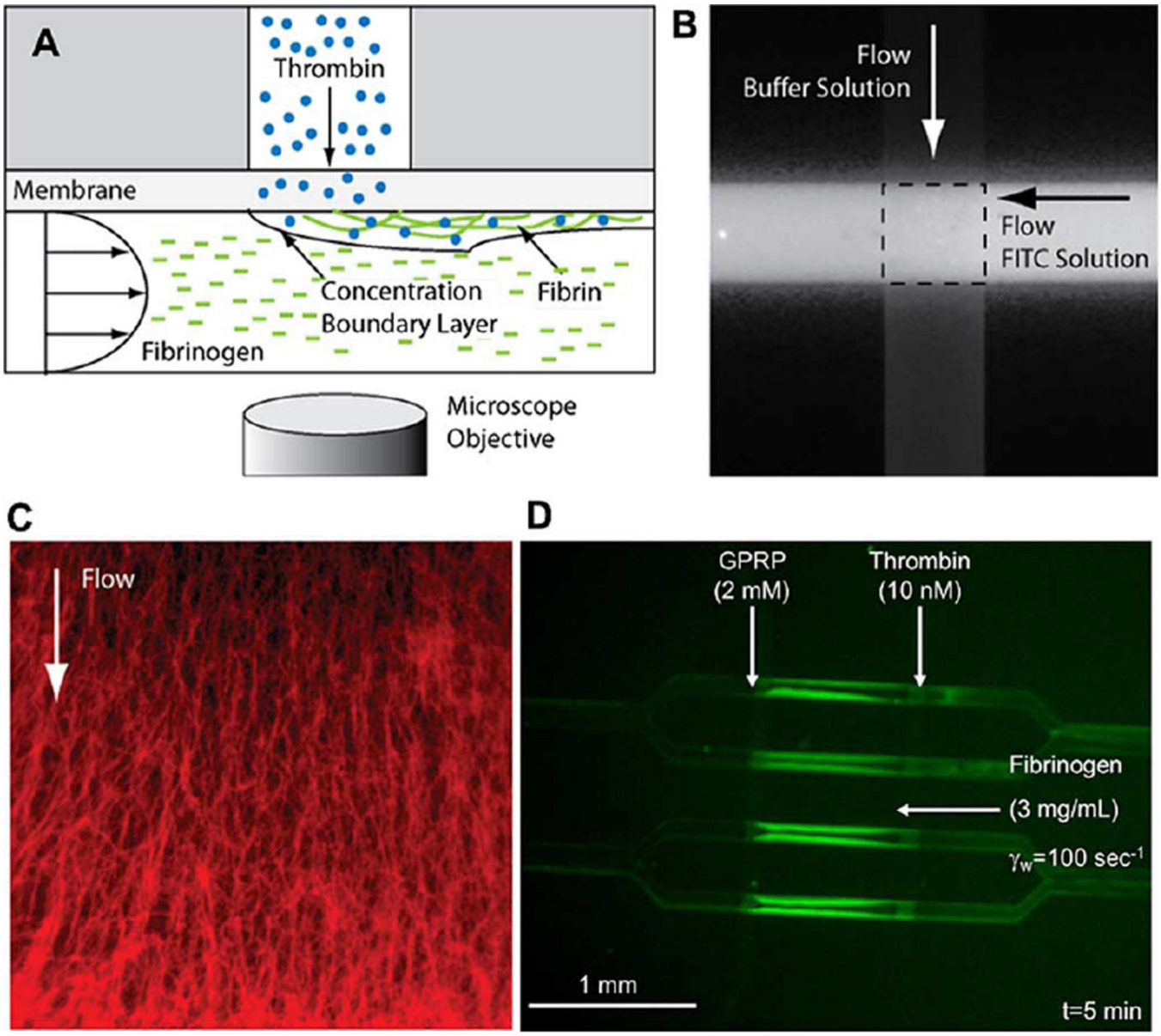

Fig. 3.

Membrane-flow device. (A) The device consists of two microfluidic channels oriented perpendicular to each other and separated by a polycarbonate membrane (pore size = 0.4 μm). Fibrinogen is perfused through the bottom channel at a desired wall shear rate. Thrombin is introduced into the flowing fibrinogen at a controlled flux. Fibrinopeptides are cleaved from fibrinogen within the thrombin concentration boundary layer, followed by fibrin monomers assembling into fibrin. The progression of fibrin formation is monitored by epifluorescence microscopy. (B) FITC is used as a tracer molecule to measure flux through the membrane prior to introduction of fibrinogen and thrombin. In the bottom channel (vertical), Tris buffered saline is flowing at a wall shear rate of 50 s^{-1}. In the top channel running horizontal, FITC (100 mM) is perfused at slightly higher hydrostatic pressure so that there is a pressure gradient that directs fluid from the top channel into the bottom

channel. The fluorescent signal downstream from the intersection of the channel (dotted lines) shows the flux of FITC into the flowing buffer solution. (C) Fibrin fiber formed during an experiment with fibrinogen flowing at a wall shear rate of 100 s^{-1} and thrombin flux of 1×10^{-20} mol/μm^2s. (D) Fibrinogen was perfused at a wall shear rate of 100 s^{-1} and thrombin was introduced at a physiological molar flux of 1×10^{-16} mol/μm^2s. Downstream fibrin polymerization was inhibited by introduced GPRP. (Colors are visible in the online version of the article; http://dx.doi.org/10.3233/BIR-15065.)

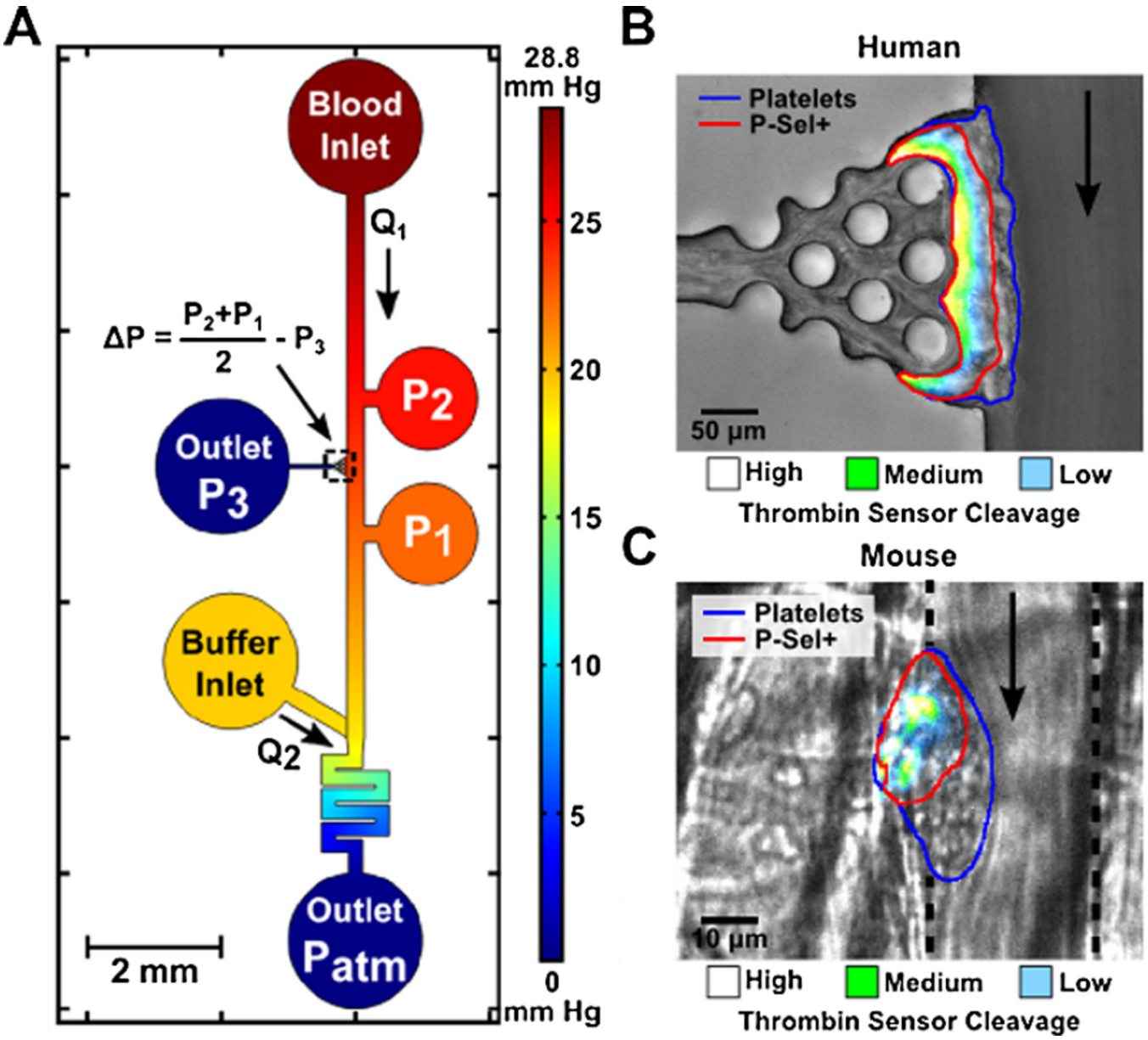

Fig. 4.

Side-view device. A microfluidic device was designed to independently control both blood pressure and shear rate at a localized site of platelet and coagulation activation (A). The device utilized a LabVIEW controlled downstream pump to control channel pressure and a user controlled upstream pump to control wall shear rate. Within the device was a post array designed to fill with collagen ± TF. This enabled studies designed to understand the spatial and temporal growth of clots at controlled hemodynamics. Human thrombi developed in the presence of a pressure differential across the injury site revealed thrombin and activation gradients that mimicked clots developed *in vivo* (B) and (C). (Colors are visible in the online version of the article; http://dx.doi.org/10.3233/BIR-15065.)

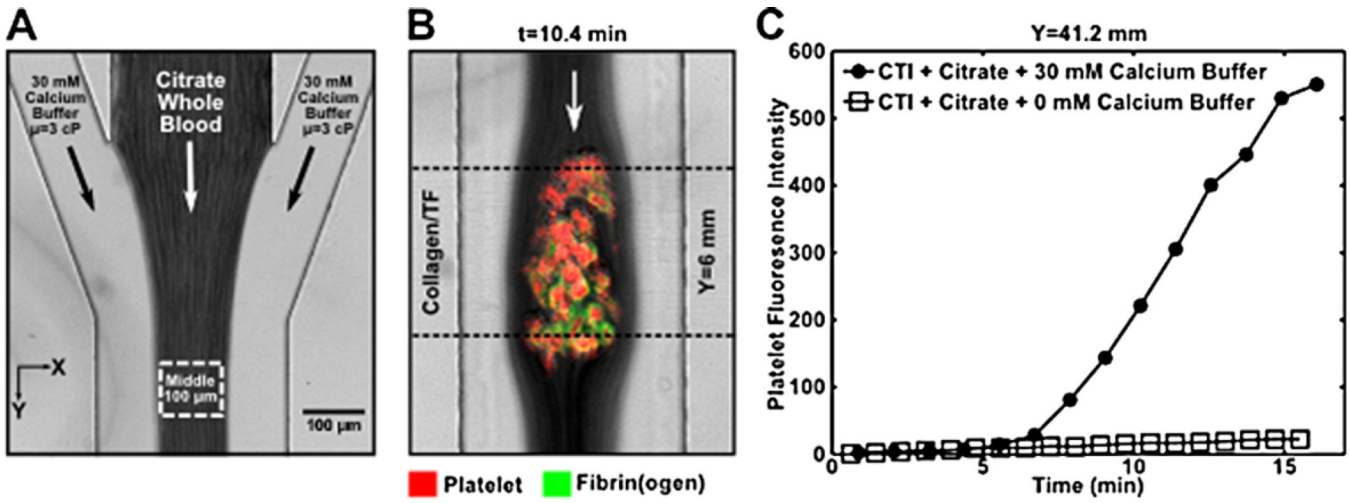

Fig. 5.

Trifurcated device. A trifurcated microfluidic channel facilitated both rapid and repeatable recalcification of citrated whole blood at a controlled shear rate (A). This enabled investigations of platelet and coagulation function downstream of the trifurcated entrance where collagen ± TF were patterned perpendicular to the flow (B). The distance (Y) to the patterned collagen strip changes the time and concentration of recalcification. Calcium buffer is required for proper platelet and fibrin (ogen) function (C). (Colors are visible in the online version of the article; http://dx.doi.org/10.3233/BIR-15065.)

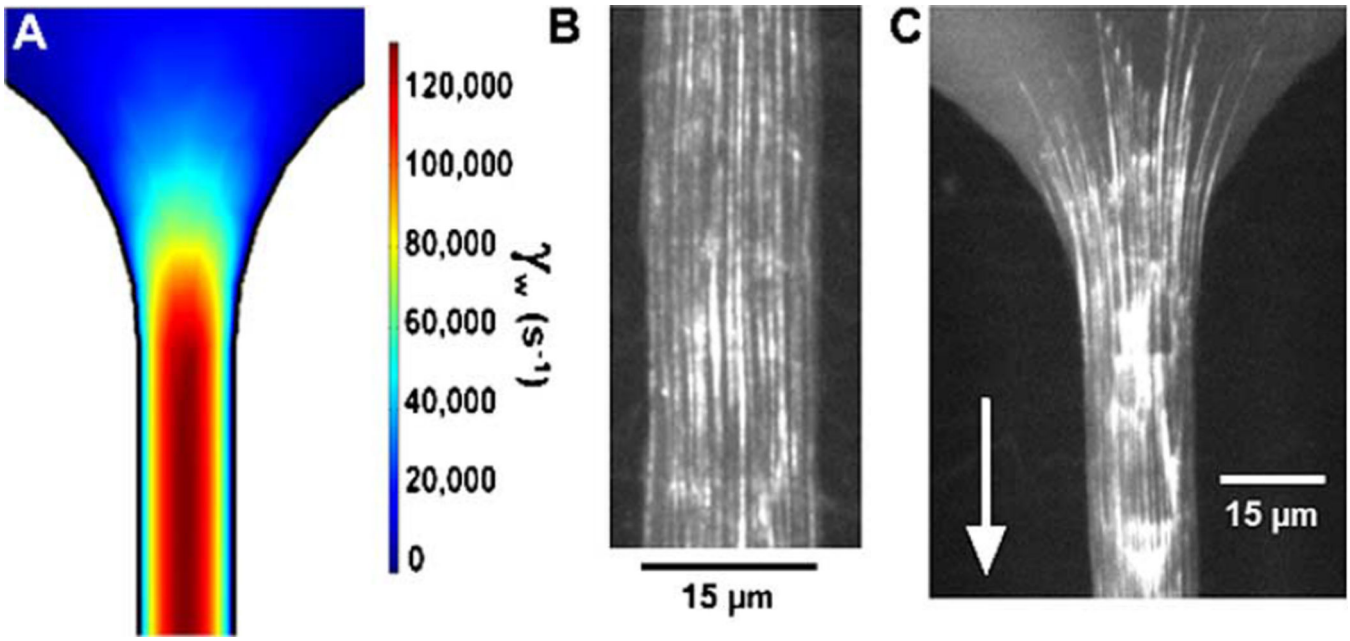

Fig. 6.

Stenosis device. Two-dimensional COMSOL model of the entrance to the stenosis region in a microfluidic stenosis model (A). Long strands of VWF deposit onto a collagen surface in the stenosis region of a microfluidic chamber perfused with platelet free plasma. Channels were post-stained with fluorescently labeled anti-VWF (B). Fibers of VWF appear in the stenosis throat region (C) where local wall shear rates are substantially higher than those in the entrance region as shown in the COMSOL model (A). (Colors are visible in the online version of the article; http://dx.doi.org/10.3233/BIR-15065.)

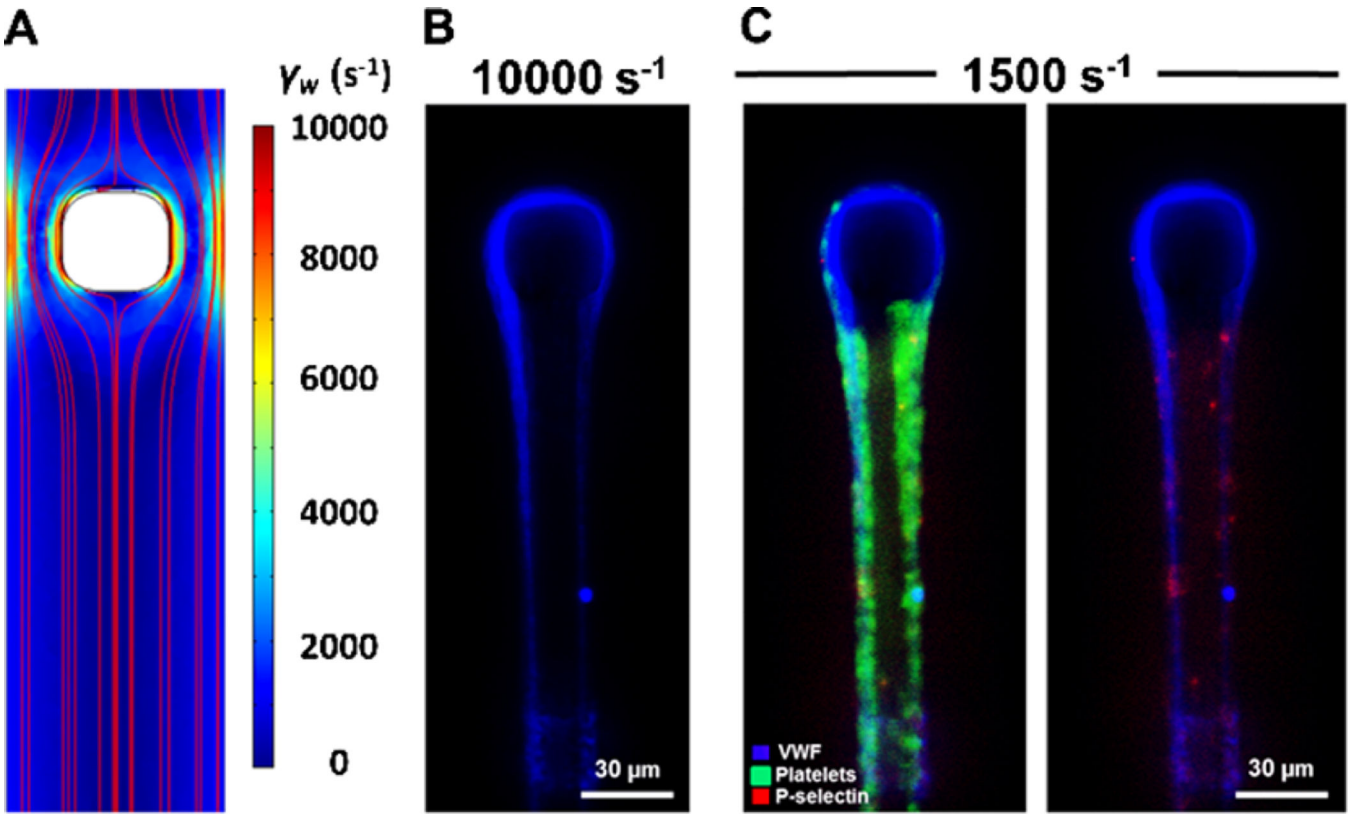

Fig. 7.

Micropost-impingement device. A microfluidic device was designed to shear plasma and capture VWF fibers without the use of collagen. The shear rates around the micropost were calculated using COMSOL (A). Perfusion of platelet-free plasma through the device at an upstream shear rate of 10,000 s^{-1} resulted in capture of VWF fibers on the micropost, which were then labeled using a FITC-conjugated anti-VWF antibody (B). Perfusion of whole blood inhibited with PPACK and apixaban over already-formed VWF fibers results in platelet adhesion, rolling, and activation on the surface of VWF. P-selectin exposure was used as a marker of platelet activation (C). (Colors are visible in the online version of the article; http://dx.doi.org/10.3233/BIR-15065.)